ELSEVIER

Ceramics International 30 (2004) 571–577

CERAMICS INTERNATIONAL

www.elsevier.com/locate/ceramint

Sintering mechanisms of ZrO_2·MgO with addition of TiO_2 and CuO

R.S. Nasar [a,*], M. Cerqueira [a], E. Longo [b], J.A. Varela [c]

[a] *Departamento de Química, UFRN, Natal, RN 59072-970, Brazil*
[b] *Departamento de Química, UFSCar, São Carlos, SP 13565-905, Brazil*
[c] *Instituto de Química, UNESP, Araraquara, SP 14800-900, Brazil*

Received 20 February 2003; received in revised form 15 April 2003; accepted 18 August 2003

Abstract

Substitutions of Ti and Cu in ZrO_2·MgO (Z), cause transformation from monoclinic (m) to cubic (c) and tetragonal (t). According to the vacancy model and solid solution formation models, neither CuO nor TiO_2 cause zirconia stabilization, which derives from other phenomena. Data analysis by TMA using the CRH (constant rate of heating) method shows a solid state reaction of ZrO_2·MgO·TiO_2 (Z·TiO_2) demonstrating a dominant mechanism of volume diffusion ($n = 1$). However, the sintering of ZrO_2·MgO·CuO (Z·CuO) shows a viscous flow mechanism ($n = 0$), a similar phenomena to that of by sintering of glass. Transformations, such as: CuO to Cu_2O at 1000 °C, ZrO_2 (m) to ZrO_2 (t) at 1100 °C and Cu_2O (s) to Cu_2O (l) at 1230 °C cause successive rearrangements of microstructure inside of region I (sintering process) and lead to interpretation errors when the Bannister equation is used.
© 2003 Elsevier Ltd and Techna Group S.r.l. All rights reserved.

Keywords: A. Sintering; D. ZrO_2; D. MgO; Zirconia stabilization

1. Introduction

Bannister developed a sintering equation [1], based on the Frenkel theory [2], that describes viscous sintering of glass. Modifications occurring at a constant heating rate (CRH) ($a = dT/dt$) are considered to be due to higher accordance with industrial sintering conditions.

Using models and examining only the initial stage of sintering [3,4] no dominant mechanism leading to densification has been observed. In region I of sintering grain rearrangement and neck formation are occurring. Mechanisms such as evaporation–condensation and surface diffusion [5] are believed to not lead to densification of ceramic compounds. However, other diffusion mechanisms are taken into account between 5 and 10% shrinkage. Research about zirconia stabilization shows similar results [6]. Grain boundary and surface diffusion are observed as the dominant densification mechanisms.

Investigations of Young and Cutler [3] into sintering of ZrO_2·Y_2O_3 with addition of TiO_2 performed by using CRH method, showed a dominant mechanism of grain boundary diffusion at the initial sintering stage. A study on initial stages of sintering of ternary system based on ZrO_2·MgO·ZnO [7] showed a mechanism of volume diffusion. Therefore, incoherent results have been obtained by using models and examining only the initial stage of sintering.

Frenkel, working with glass, demonstrated a viscous flow behavior due to diffusion of atoms or ions into the crystal structure. The influence of microstructure on the sintering process is not explained sufficiently by the Frenkel model.

Kuczynski [8] developed a model based on atom and ion diffusion by vacancies. Such a model considers a decrease of surface area due to diffusion of ions in regions between particles from a large to a small curvature ratio (neck).

Grain boundaries of particles have high concentrations of defects such as incomplete bonding, and the presence of vacancy and dislocations. Coble [9] developed a model considering that the grain boundaries exchange mass with the neck between particles, due to high concentration of vacancies on the particle boundaries. Modifications of such a model permitted the analysis of sintering under isothermal conditions and at constant heating rates.

Coble proposed modification in the CRH model and assumed that small grain growth is occurring at the initial sintering stage. Simultaneous mechanisms are not considered by the Bannister equation.

* Corresponding author. Tel.: +55-84-215-3823; fax: +55-84-211-9224.
E-mail address: nasar@terra.com.br (R.S. Nasar).

0272-8842/$30.00 © 2003 Elsevier Ltd and Techna Group S.r.l. All rights reserved.
doi:10.1016/j.ceramint.2003.08.005

Table 1
Origin of reagents, purity, particle size (P.S., μm), and surface area (S.A., m^2/g)

	Origin	Purity	P.S. (μm)	S.A. (m^2/g)
ZrO_2	IPEN	99.9	1.80	5.2
MgO	Vetec	99.8	1.10	2.8
TiO_2	Riedel-Hagen	99.9	0.84	5.6
CuO	Vetec	99.9	0.67	3.3

The subject of this work is the analysis of two sintering conditions applying the Bannister equation, such as a solid–solid reaction that uses vacancies for a mass transport of ZrO_2·MgO·TiO_2, and a presence of liquid phase in ZrO_2·MgO·CuO. An analysis and a discussion of the sintering model are carried out.

2. Experimental procedures

2.1. Powder processing

High purity materials (Table 1) are used for the processing of both CuO and TiO_2 in Z·M (0.25 mol%). The surface area was analyzed by using an ASAP 2000 (BET method) and the particle size distribution using a Micromeritics Sedigraph.

Raw materials were grinded by friction for 1 h and mixed for 4 h with ethyl alcohol. The powder was dried, deagglomerated in an alumina mortar, sieved on 325 meshes and pressed uniaxially and isostatically at 100 and 150 MPa, respectively. The ceramics were sintered at different heating rates using a thermal mechanical analyser (TMA).

2.2. CRH method and Bannister equation

Constant heating rates of 5, 10, 15 and 20 °C/min from 100 to 1600 °C at atmospheric pressure were applied. In sintering region III (final sintering stage) the furnace was cooled from 1600 °C to ambient temperature and the apparent density was measured by using the Archimedes method. The ceramic material was analysed using a Netzsch dilatometer Model 402 E.

According to Bannister:

$$\mathrm{d}\left(\frac{\Delta L/L_0}{\mathrm{d}t}\right) = \frac{\kappa}{(\Delta L/L_0)_n} \tag{1}$$

where $\Delta L/L_0$ = shrinkage at sinterization; L = final length of sample; L_0 = initial length of sample; $\mathrm{d}t$ = time differential; $\kappa = \kappa_0 \exp(-E_a/RT)$ = velocity constant t; $a = \mathrm{d}T/\mathrm{d}t$ = constant rate of heating; n = mechanism of sintering.

A rearrangement of Eq. (1) gives,

$$\left(\frac{\Delta L}{L_0}\right)^n = \left[\frac{(n+1)}{a}\right] \int_{t_o}^{t} \kappa_0 \exp\left(\frac{-E_a}{RT}\right) \mathrm{d}T \tag{2}$$

If E_a is much better than RT, then:

According to Bannister and other authors [7],

$$\left(\frac{\Delta L}{L_0}\right)^{n+1} = -aC^* \tag{3}$$

C^* = constant

Applying a log function for both terms, one obtains:

$$(n+1)\ln\left(\frac{\Delta L}{L_0}\right) = -\ln a + \ln C^* \tag{4}$$

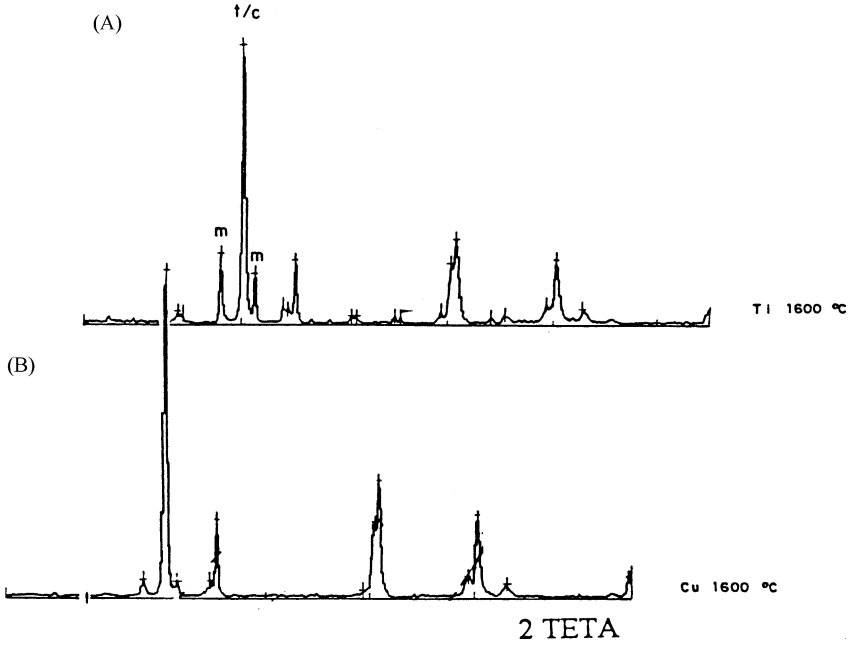

Fig. 1. X-ray diffraction pattern (XRD) of (A) Z·M·TiO_2 and (B) Z·M·CuO, sintered up to 1600 °C.

$$\ln\left(\frac{\Delta L}{L_0}\right) = -\left(\frac{1}{n+1}\right)\ln a + \frac{\ln C^*}{n+1} \quad (5)$$

A graph, such as $\ln \Delta L/L_0$ against $\ln a$, with a gradient of $(-1/n+1)$, or $\ln a$ against $\ln \Delta L/L_0$, with a gradient of $-(n+1)$, may be plotted.

2.3. Phase analysis

The Rietveld [10] method was applied using step by step scanning with a constant increment and time of measuring. For valid overlap between two or more peaks:

$$Y_{ec} = S\sum_h L_h |F|_h^2 \phi(\Delta 2\Theta i_h) P_h + yb_i \quad (6)$$

Where: Y_{ec} = total peak contribution; S = scale factor; L_h = Lorentz and polarization factor and multiplicity; P_h = preferred orientation function; F_h = structure factor; $\Delta 2\Theta_i$ = reflection profile function; yb_i = next peak contribution.

Deconvolution of diffraction peaks and phase analysis by the Rietveld method was carried out. An approximation between points of an observed X-ray diffraction analysis y(o) and a calculated XRD pattern y(c), was done by least squares as shown in the following:

$$F_M = \sum_{i-1}^{N} W_1 \langle y_i(o) - y(c)\rangle^2 \quad (7)$$

$(W_i)^{-1} = \sigma_i^2 =$ standard deviation on total intensity

2.4. SEM analysis

Samples sintered up to 1600 °C at different heating rates were polished by using 0.1 and 1 μm alumina and with 2 and 5 μm diamond, respectively. Chemical attaches with HCl/ethyl alcohol 5 vol.% for 20 s show the contours of microstructure. Gold was deposited by sputtering over the sample surface and a microscopy analysis was carried out immediately with a model JEOL JSM-T 330 A at magnifications of up to 10,000 times. The average quantity of phases and grain sizes was calculated according the ASTM standard.

3. Results

3.1. Phase analysis and linear shrinkage

Fig. 1 shows the X-ray diffraction pattern (XRD) of powder sintered at 1600 °C/2 h with heating rate of 10 °C/min in ambient atmosphere. Increases of phases of partially stabilized zirconia (PSZ) [11] were observed for TiO_2 and CuO additions. Three phases of ZrO_2, such as monoclinic (m), tetragonal (t) and cubic (c), were observed by deconvolution of X-ray diffraction peaks.

Table 2
Phase quantity of Z·M (ZrO_2·MgO), Z·TiO_2 (ZrO_2·MgO·TiO_2) and Z·CuO (ZrO_2·MgO·CuO)

Material	Monoclinic (%)	Tetragonal (%)	Cubic (%)
Z·M	36.1	3.2	60.7
Z·TiO_2	33.0	30.0	37.0
Z·CuO	6.4	81.6	12.0

Analysis of ZrO_2·MgO (Z·M) phases (Table 2) shows 60.7% of stabilization of cubic phase. The phase quantity of Z·CuO, (ZrO_2·MgO·CuO) shows transformations from c phase to t with high increase of stabilized phases. However, TiO_2 additions caused small contributions to the stabilization effect. Systems based on CaO and MgO in binary mixtures with ZrO_2 [12,13] lead to c-ZrO_2 stabilization (TSZ). Such results do not agree with the model that considered the ZrO_2 stabilization, caused by only ion formers of substitution solid solution.

Fig. 2 shows a rapid shrinkage of Z·TiO_2 (ZrO_2·MgO·TiO_2) during sintering at rates of 5 and 10 °C/min close to 904 °C (region I). The Z·CuO shows a slow shrinkage from 900 to 1340 °C. Three phase transformations, such as from CuO to Cu_2O at 1000 °C/2 h (region I), ZrO_2 phase transformation from m phase to t at 1100 °C (near by region II), and liquid phase formation of Cu_2O close to 1230 °C/2 h (region II) is occurring [14]. Various transformations cause microstructure rearrangements up to 1290 °C/2 h. The shrinkage, of both systems, inside of intermediary region (region II) demonstrates different stages of densification at the same temperature. However, in the end region of

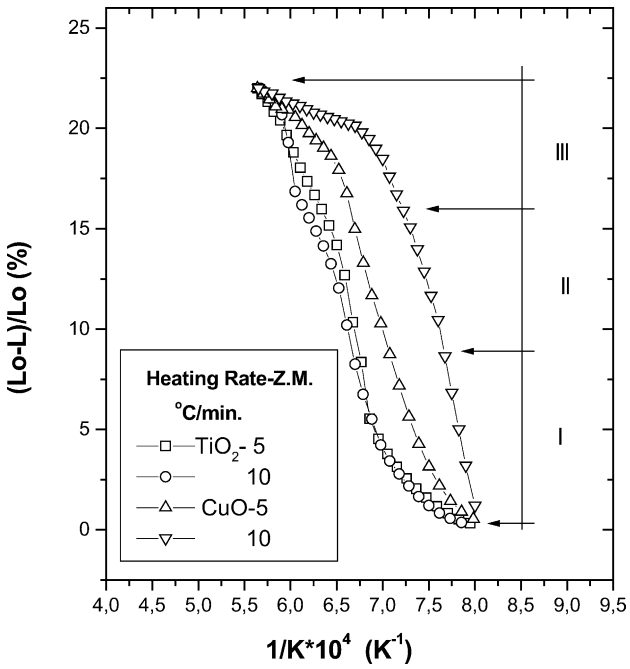

Fig. 2. Shrinkage of Z·TiO_2 and Z·CuO with heating rates of 5 and 10 °C/min.

sintering (region III) coincident points are observed at different heating rates. Applications of the Bannister equation on experimental data are valid only at the initial stage of sintering due to avoiding grain growth that causes deviations from the theoretical model.

3.2. Density and grain growth

Fig. 3 shows a rapid densification of Z·TiO_2 from 3.5 g/cm^3 at 800° to 5.4 g/cm^3 at 1600 °C, respectively. Two steps of rearrangements during the densification of Z·CuO occurred, first by the CuO–CuO_2 transformation close to 1000 °C, and second during a liquid phase formation close to 1230 °C.

Densities, of about 5.65 g/cm^3 at 1400 °C/2 h and 5.42 g/cm^3 above 1500 °C/2 h show that a loss of Cu_2O leads to decreases in the density of Z. Transformations in the region I of the sintering process (close to region II) show reverse tendency of densities between Z·TiO_2 and Z·CuO (Fig. 3).

Fig. 4 shows the slow grain growth at low temperature for both titanium oxide and cupper oxide additions. After 1400 °C an exponential growth is observed with formation of large grain sizes. Liquid phase during sintering caused increase of average size of grains.

In the regions II and III rearrangements of microstructure and a dissolution–precipitation process occur. High microstructure homogeneity due to a mass transport of liquid phase, which cause a rapid grain growth at high temperatures was observed.

3.3. Sintering mechanism and microstructure

SEM observations of samples of TiO_2 and CuO-doped Z·ZrO_2 sintered at 1500 °C/2 h (Fig. 5A and B) show incomplete grain formation and a presence of high residual porosity for both systems. The evidence of a neck formation in the Z·CuO sintering process (1500 °C) and small grains in the Z·TiO_2 microstructure demonstrate that high temperature is necessary for a complete sintering process.

High grain growth from 1500 to 1600 °C/2 h, is observed for both systems (Fig. 5C and D); however, an abnormal grain growth in the Z·CuO due to a large particle size distribution occurs. In the region III does not occurs remnant liquid phase of Cu_2O demonstrating that at the end stage of the sintering process a solid state reaction is occurring.

Calculations of sintering mechanism of Z·TiO_2 (Fig. 6A) show n values from 1.009 ($n = 1$) at 1040 °C to 9.32 at 1120 °C (region I). According to the Bannister equation there is occurring a volume diffusion type mechanism. Above 1060 °C a deviation due to microstructure effects show incoherent results. Activation energy calculated for sinterization was about 462.7 ± 17 kJ/mol.

The n values (Fig. 6B) observed during the sintering of Z·CuO are between 0.12 at 1010 °C and 0.028 (∼0) at 1070–1130 °C (region I), characterizing a viscous flow type mechanism. Such a mechanism, according the Frenkel model occurs only in glass sintering. These phenomena could be attributed to different stages of rearrangement of the microstructure with successive accommodations and tension relief between the grains. The observed activation energy of 438 ± 8.8 kJ/mol, beeing lower than that obtained for the Z·TiO_2 system.

4. Discussion

Addition of CuO and TiO_2 increased the stabilized phases of Z. Some authors accept only solid solution formation and vacancy creations [15] as principal causes of zirconia stabilization. According to the conclusion of the Hume-Rothery rule [16], NBS researchers [17] and Dietzel and Tober [18],

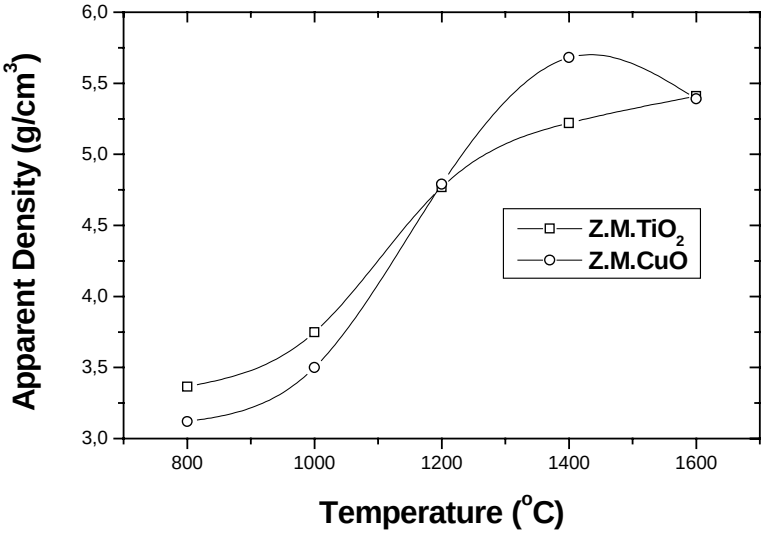

Fig. 3. Apparent density (g/cm^3) against temperature of Z·TiO_2 and Z·CuO from 800 to 1600 °C.

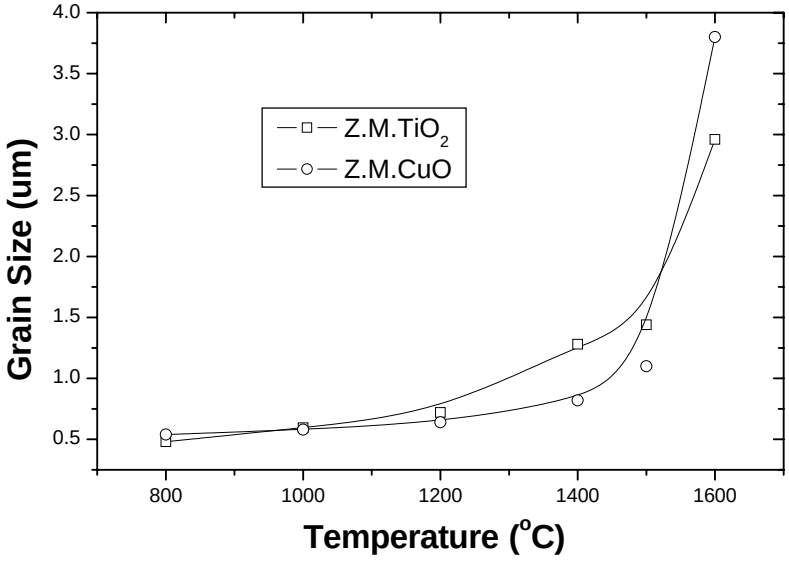

Fig. 4. Grain size (μm) against temperature of Z·TiO_2 and Z·CuO from 800 to 1600 °C.

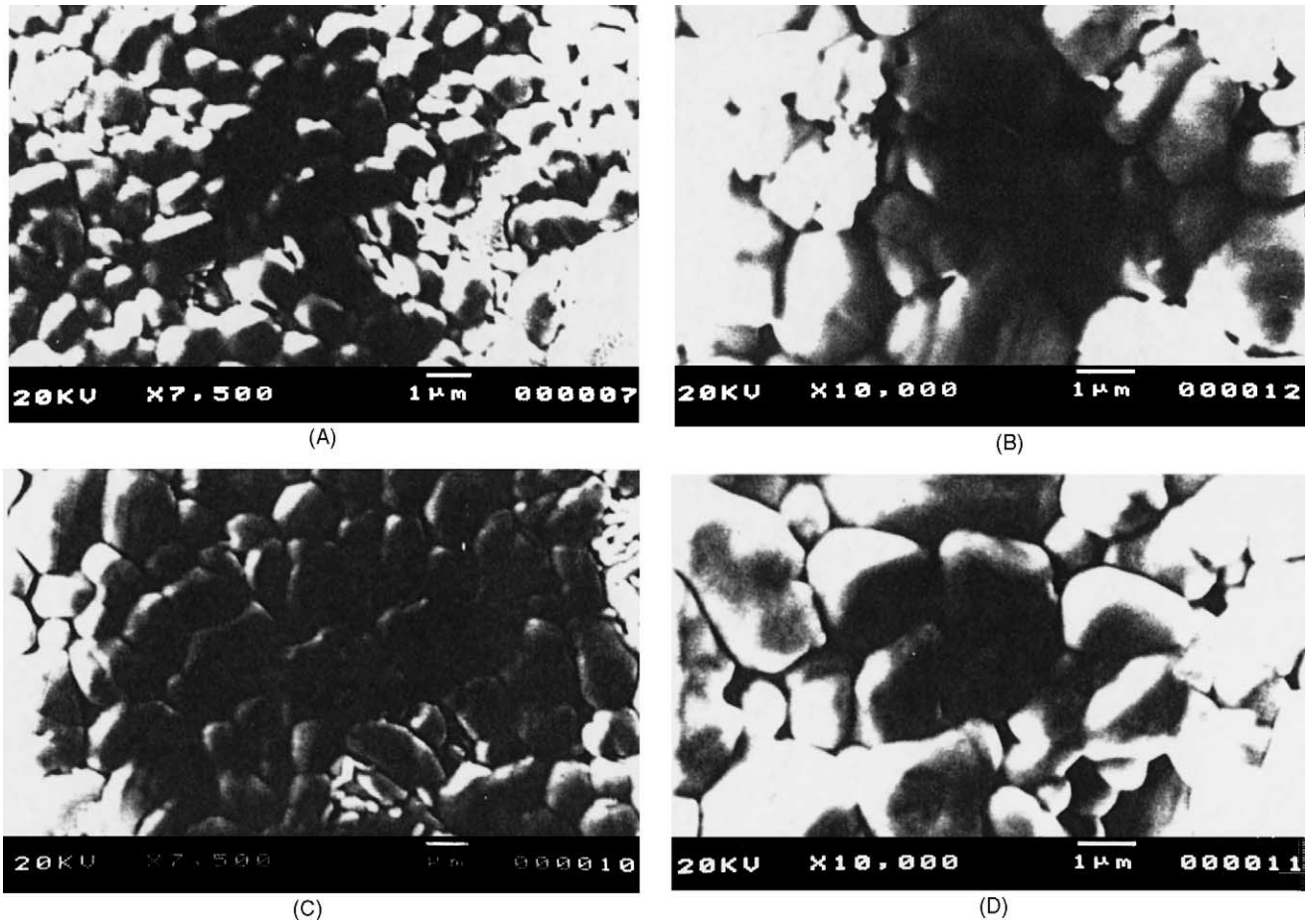

Fig. 5. Microstructure analysis by SEM: (A and C) Z·TiO_2 sintered at 1500 °C and 1600 °C/2 h, respectively; (B and D) Z·CuO sintered at 1500 °C and 1600 °C/2 h, respectively.

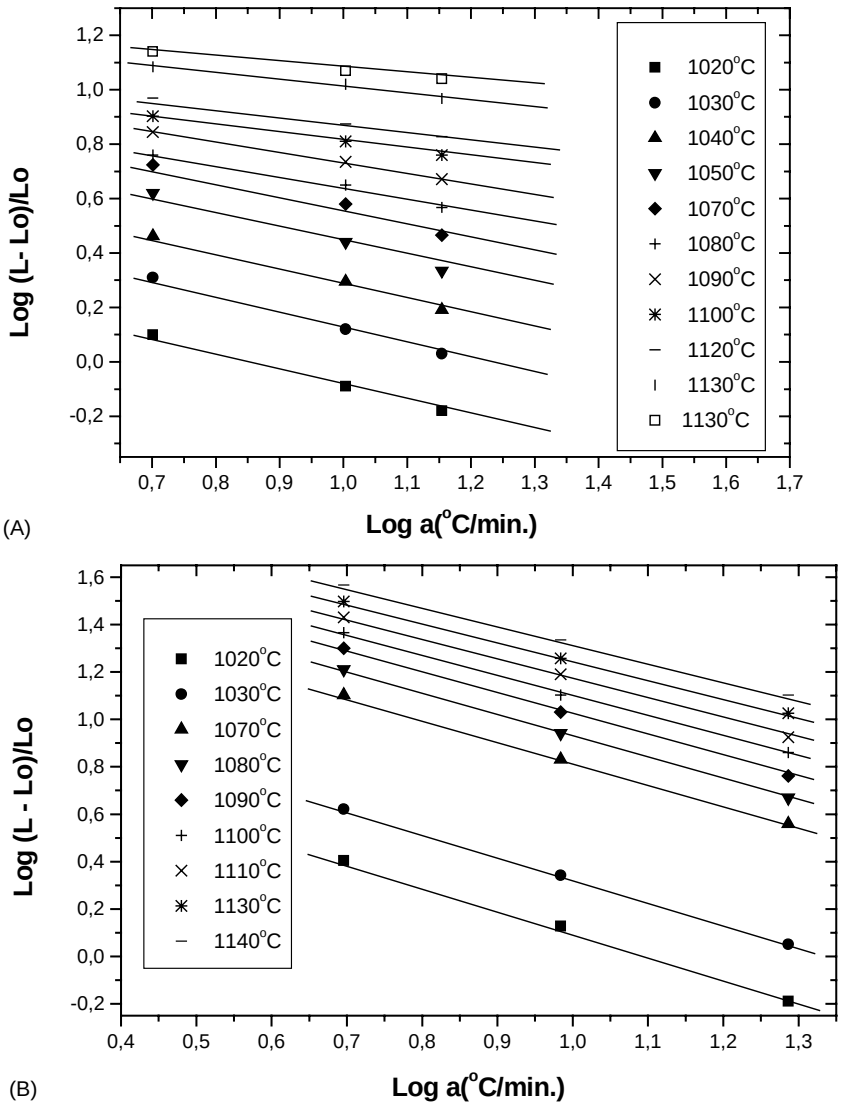

Fig. 6. Mechanism of sintering: (A) Z·TiO_2, (B) Z·CuO.

MgO led to stabilization of ZrO_2 with t and c phases. A mechanism of structure electroneutrality causes the formation of oxygen vacancies through reactions of the type:

$$\mathrm{MgO} \xrightarrow{\mathrm{ZrO_2}} \mathrm{Mg''_{Zr}} + V_{\ddot{O}} + \frac{1}{2}\mathrm{O_2} \quad (8)$$

However, additions of TiO_2 or CuO on binary mixtures does not cause zirconia stabilization according to those models proposed and accepted above. Nevertheless, the addition of titanium oxide to a ternary system increased the ZrO_2 stabilization without vacancy formation, and copper preferentially led to t-ZrO_2 (Fig. 2). All substitutions in the ZrO_2 structure [12,13] occurred by solid state reactions. However, before a solid state reaction there is a liquid phase formation of Cu_2O.

$$\mathrm{TiO_2} \xrightarrow{\mathrm{ZrO_2}} \mathrm{Ti^X_{Zr}} + \frac{1}{2}\mathrm{O_2} \quad (9)$$

The vacancy brings local tensions of the lattice into relief and increases the phase stability. However, it is a consequence of electroneutrality between charges and not the only reason for the stabilization effect. These data led to a different interpretation by other authors, who consider hybrid orbital formation as a reason for the zirconia stabilization [14]. Reactions of TiO_2 as well as CuO occurred on the solid state (region I), (Fig. 2) by interfaces of diffusion of ZrO_2/MgO and ZrO_2/CuO. Near to region II, at about 1230 °C (intermediary stage of the sintering), the liquid phase formation of copper oxide did not cause deviation between theoretical and experimental results when only 5% of shrinkage was considered in the analysis (<1100 °C, inside of region I). The grain growth of the Z·TiO_2 (Fig. 5) initiating at 1025 °C (region I), was coincident with an increase of apparent density near to 1000 °C (~975 °C), and due to this, above 1060 °C incoherent values of *n* were obtained. A slow diffusion process occurred by a solid state

reaction which depends on vacancy concentration. Due to a high coordination between Zr and Ti ions small quantities of $ZrTiO_4$ could occur causing a decrease of zirconia stabilization.

Close to 1000 °C and between 1100 and 1200 °C, both systems showed an evidence of a rearrangement process and mass distribution by solid state reaction and after 1250 °C only a change of density of Z·TiO_2 and Z·CuO was observed. During the sintering (region II) a Z·CuO liquid phase formation led to solution-precipitation that caused a mass transport on the grain boundaries of microstructure, small grains were dissolved and the mass was transported throughout the microstructure. A different kinetic effect occurred with the addition of TiO_2 and a solid–solid diffusion process, which demonstrated a decrease of densification between the regions II and III of sintering process take place. This is evidenced by a rapid shrinkage (1000–1290 °C), an increase of apparent density (1000–1425 °C) and grain growth above 1025 °C.

The Z·CuO shows densities of 5.7 g/cm^3 at 1400 °C and 5.4 g/cm^3 at 1600 °C and the Z·TiO_2 mixture shows densities of 5.25 g/cm^3 at 1600 °C likely due to the formation of an intermediary phase, $ZrTiO_4$ near to 1400 °C which caused a competition with the diffusion process of MgO in ZrO_2.

Such complexity could require an additional energy in the densification process (462.7 kJ/mol).

Mechanisms, such as volume diffusion showed by Z·TiO_2 analysis, caused densification of ceramic body. However, in the sintering region I, other mechanisms could occur, such as overlapping of a surface diffusion and/or evaporation–condensation, which did not lead to densification (neck formation). However, only a slower rate control process is observed.

In the region I errors of contour conditions of the Bannister equation (caused by kinetic of grain growth above 1030 °C) do not occur. Above 1100 °C (region II) and in the region III strong shrinkage and grain growth led a deviation between experimental data and Bannister equation applications. Studies of the sintering mechanism of Z·ZnO showed the same results [7].

According to the Frenkel model of sintering there is a viscous flow mechanism only during sintering of glass. Such phenomena led to interpretation errors of the Bannister equation, which could be explained by different stages of rearrangements.

Two transformations, such as from CuO to Cu_2O at 1000 °C (region I) that caused alteration of the unit cell volume and a transformation from m to t-ZrO_2 (end of region I) promoted rearrangements of microstructure.

Phase transformation from 1000 to 1230 °C is effectively an event of successive rearrangements. Thus, various sequential rearrangements showed a similar behavior to a viscous flow effect [2]. Increases of shrinkage and apparent density between 890 and 1290 °C with small grain growth reinforced the occurrence of different stages of rearrangements in the microstructure. Between 970 and 1040 °C does not occur influence of ZrO_2 phase transformation (close to 1100 °C) and of a liquid phase formation above 1230 °C. Rapid rearrangements of microstructure at the initial stage of sintering caused interpretation errors of the Bannister equation. However, this model is appropriate for solid state reactions, like volume diffusion and grain boundary diffusion mechanisms.

5. Conclusions

Additions of CuO and TiO_2 in Z increase the stabilized phases of ZrO_2 despite models that accept only a solid solution formation and vacancy creation as reasons for stabilization. A mechanism of volume diffusion ($n = 1$) occurs in the Z·TiO_2 sintering and shows an increase of densification during sintering (region I). However, three transformations on the Z·CuO sintering occur, namely: Transformations from CuO (s) to Cu_2O (s) at 1000 °C, from ZrO_2 (m) to ZrO_2 (t) at 1100 °C and a liquid phase formation from Cu_2O (s) to Cu_2O (l) at 1230 °C. Such transformations shows a viscous flow mechanism ($n = 0$) typical of glass sintering. The phenomenon was attributed to various microstructure rearrangements caused by the phase transformations during sintering.

Acknowledgements

Financial support from the research funds of CNPq is gratefully acknowledged.

References

[1] M.J. Bannister, J. Am. Ceram. Soc. 51 (10) (1968) 548.
[2] J. Frenkel, J. Phys. (USSR) 9 (5) (1945) 385.
[3] W.S. Young, Y.B. Cutler, J. Am. Ceram. Soc. 53 (12) (1970) 659.
[4] A. Ikesue, S.-I. Matsuda, S.-J. Shirasaki, Taikabutsu Overseas 12 (3) (1991) 12.
[5] Y.-M. Chiang, D. Birnie III, W.D. Kingery, Physical Ceramics—Principles for Ceramic Science and Engineering, Wiley, USA, 1997.
[6] W.H. Rhodes, J. Am. Ceram. Soc. 64 (1) (1981) 19.
[7] R.S. Nasar, M. Cerqueira, E. Longo, J.A. Varela, Ceram. Int. 25 (1999) 593.
[8] G.C. Kuczynski, I. Zaplatynskyj, J. Am. Ceram. Soc. 39 (10) (1956) 349.
[9] R.L. Coble, J. Am. Ceram. Soc. 41 (1) (1958) 55.
[10] H.M. Rietveld, J. Appl. Crystallogr. 2 (1969) 65.
[11] R.A. Cutler, J.R. Reynolds, A. Jones, J. Am. Ceram. Soc. 75 (8) (1992) 2173.
[12] E.K. Koehler, Ceram. Int. 10 (1984) 3.
[13] E.K. Koehler, Ceram. Int. 11 (1985) 3.
[14] R.S. Nasar, Dr. Thesis, UFSCar, São Carlos-SP, Brazil, 44 pp., 1994.
[15] N. Claussen, R. Wagner, L.J. Gauckler, G. Petzow, J. Am. Ceram Soc. 61 (7/8) (1978) 169.
[16] W. Hume-Rothery, in: J.F. Shackelford (Ed.), Introduction to Materials Science for Engineers, MacMillan, New York, 1985, p. 127.
[17] L.W. Coughanour, R.S. Roth, S. Marzullo, F.E. Sennet, J. Res. Nat. Bur. Standards 54 (4) (1955) 191–199. RP2580.
[18] A. Dietzel, H. Tober, Ceram. Abstr. 1954, 23a.